CSCanada
Advances in Petroleum Exploration and Development
Vol. 6, No. 1, 2013, pp. 69-74
DOI:10.3968/j.aped.1925543820130601.1658

ISSN 1925-542X [Print]
ISSN 1925-5438 [Online]
www.cscanada.net
www.cscanada.org

The Research of Reverse-Time Migration for Cross-Hole Seismic

LI Zhe[a]; CAO Xia[b]; LIN Songhui[c]; WEI Guohua[c]

[a] College of information and control engineering, China University of Petroleum (East China), Qingdao, China.
[b] School of Geosciences, China University of Petroleum (East China), Qingdao, China.
[c] Shengli Geophysical Research Institute of SINOPEC, Dongying, China.
*Corresponding author.

Received 6 August 2013; accepted 25 September 2013

Abstract
Cross-hole seismic is the leading technology of development seismology, which is still developing and improving. With the development of down-hole acquisition equipment, cross-hole seismic acquisition technology is getting mature, providing better data for imaging. According to the features of cross-hole survey and cross-hole data, we put forward a reverse-time migration method which is suitable for the wave equation for cross-hole seismic data. We propose finite difference scheme of higher order, and then derive its stability condition in cross-hole seismic. The frequency dispersion problem in cross-hole seismic wave field extrapolation is also discussed. Cross correlation imaging condition is used to realize migration, and Laplace filter is applied to remove low-frequency noise from migration section. Thus finite-difference reverse-time migration method for cross-hole seismic is established. Finally, we build geological models with anomalous ellipsoids, and apply cross-hole seismic wave field simulation and migration to them, thus our method proves its effectiveness. When dealing with real cross-hole seismic data with this method, high-resolution migration sections can be achieved.

Key words: Cross-hole seismic; Reverse-time migration; Model test

Li, Z., Cao, X., Lin, S. H., & Wei, G. H. (2013). The Research of Reverse-Time Migration for Cross-Hole Seismic. *Advances in Petroleum Exploration and Development*, *6*(1), 69-74. Available from: http://www.cscanada.net/index.php/aped/article/view/j.aped.1925543820130601.1658
DOI: http://dx.doi.org/10.3968/j.aped.1925543820130601.1658

INTRODUCTION
Cross-hole seismology has found its place in oil and gas exploration and development. It is one of the key technologies of reservoir geophysics, and is still developing and improving. Cross-hole seismic high-resolution imaging under complex structure condition has long been a bottleneck problem restricting the development and application of cross-hole seismic. Unlike surface seismic, on one hand, cross-hole seismic is applied in well-hole, thus its data has higher resolution and S/N ratio which promising a high-quality input data for seismic imaging. On the other hand, its seismic imaging is much easier implicated by direct wave and supercritical reflections, for bigger incident angles and the lack of reflections from small incident angles and zero incident angle which is caused by the closeness of source and receiver.

Reverse-time migration is firstly proposed in SEG annual conference in 1983[1]. This method solves two-way wave equation directly, and describes the transmission features of wave fields accurately. Theoretically, it can delineate underground structures precisely using full wave field information, thus is the most accurate imaging method. In several decades, a mass of studies has been done to surface seismic reverse-time migration method by geologists from all over the world[2-5]. However, Xianhua Zhu and McMechan firstly applied acoustic reverse-time imaging to post-stack cross-hole seismic data[6]. After that, some other geologists also make efforts to cross-hole seismic migration study[7-10]. Generally, the quantity of study and application of cross-hole seismic acoustic wave reverse-time migration is much smaller than that of surface seismic reverse-time migration.

In this paper, we discussed cross-hole seismic acoustic wave reverse-time migration method, the construction of difference scheme and the stability condition for deriving difference scheme, using the research results of surface seismic acoustic wave reverse-time migration as

a reference. Finally the method is applied to real seismic data, and proves its effectiveness.

1. METHOD

1.1 Cross-Hole Acoustic Wave Reverse-Time Migration

In reverse-time migration, two-way wave equation is solved directly. And the method describes the transmission features of wave fields accurately. Theoretically, it can delineate underground structures precisely using full wave field information[11].

2-D acoustic wave equation in isotropic medium is:

$$\frac{\partial^2 u}{\partial x^2}+\frac{\partial^2 u}{\partial z^2}=\frac{1}{v^2(x,z)}\frac{\partial^2 u}{\partial t^2} \tag{1}$$

where x and z are spatial point coordinates, t represents time, u(x,z,t) represents stress field and v(x,z) represents medium velocity.

Reverse-time migration is applied to seismic data as the following three steps:

(1) Set that source function is initial condition, use equation 1 to do forward extrapolation and derive the wave field at source point;

(2) Set that received seismic method record is boundary condition, use equation 1 to do reverse extrapolation and derive the wave field at receiver point;

(3) Use imaging condition to extract imaging value, according to source wave field and receiver wave field.

1.2 The Construction of Difference Scheme

Set that $u_{i,j}^n=u(i\Delta x, j\Delta z, n\Delta t)$, where i, j and n represent discrete points corresponding x, z and t separately, Δx and Δz represent spatial sampling intervals along x and z axis separately, and Δt represents time interval. The second partial derivative of u(x,z,t) with respect to x is $\frac{\partial^2 u}{\partial x^2}$, and its 2M-order central difference scheme can be approximately expressed as:

$$\frac{\partial^2 u_{i,j}^n}{\partial x^2}=\frac{1}{\Delta x^2}\sum_{m=1}^{M}a_m\left[u_{i+m,j}^n+u_{i-m,j}^n-2u_{i,j}^n\right] \tag{2}$$

where a_m is difference coefficient. When M>2, a_m can be calculated by the following equation[12]:

$$a_m=\frac{(-1)^{m+1}}{m^2}\frac{\prod_{i=1,i\neq m}^{M}i^2}{\prod_{i=1}^{m-1}(m^2-i^2)^2\prod_{i=m+1}^{M}(i^2-m^2)^2} \tag{3}$$
$$(m=1,2,\cdots,M;M>2)$$

Similarly, the 2M-order central difference scheme of u(x,z,t) with respect to z and t is expressed as the following equations:

$$\frac{\partial^2 u_{i,j}^n}{\partial z^2}=\frac{1}{\Delta z^2}\sum_{m=1}^{M}a_m\left[u_{i,j+m}^n+u_{i,j-m}^n-2u_{i,j}^n\right] \tag{4}$$

$$\frac{\partial^2 u_{i,j}^n}{\partial t^2}=\frac{1}{\Delta t^2}\left[u_{i,j}^{n+1}+u_{i,j}^{n-1}-2u_{i,j}^n\right] \tag{5}$$

Apply second order central difference scheme to temporal partial derivative, while applying 2M-order central difference scheme to spatial partial derivative, thus equation 1 can be written as:

$$\begin{aligned}u_{i,j}^{n+1}=&2u_{i,j}^n-u_{i,j}^{n-1}+\left(\frac{c\Delta t}{\Delta x}\right)^2\sum_{m=1}^{M}a_m\left[u_{i+m,j}^n+u_{i-m,j}^n-2u_{i,j}^n\right]\\&+\left(\frac{c\Delta t}{\Delta z}\right)^2\sum_{m=1}^{M}a_m\left[u_{i,j+m}^n+u_{i,j-m}^n-2u_{i,j}^n\right]\end{aligned} \tag{6}$$

Similarly, the difference scheme of reverse-time extrapolation is:

$$\begin{aligned}u_{i,j}^{n-1}=&2u_{i,j}^n-u_{i,j}^{n+1}+\left(\frac{c\Delta t}{\Delta x}\right)^2\sum_{m=1}^{M}a_m\left[u_{i+m,j}^n+u_{i-m,j}^n-2u_{i,j}^n\right]\\&+\left(\frac{c\Delta t}{\Delta z}\right)^2\sum_{m=1}^{M}a_m\left[u_{i,j+m}^n+u_{i,j-m}^n-2u_{i,j}^n\right]\end{aligned} \tag{7}$$

1.3 Stability Condition

When using equation 6 and equation 7 to do forward and reverse extrapolation, the stability condition of difference scheme must be satisfied, otherwise overflow occurs in calculation process and leads to a wrong result.

$$u(x,z,t)=u_0e^{i(wt-k_x\cdot x-k_z\cdot z)} \tag{8}$$

where u_0 is the wavelength at the starting time, and k_x and k_z are horizontal wave number and vertical wave number separately.

Use equation 8 to simplify equation 6, and then we derive:

$$\begin{aligned}2\sin^2\left(\frac{\omega\cdot\Delta t}{2}\right)=&\frac{v^2\cdot\Delta t^2}{\Delta x^2}\left\{\sum_{m=1}^{M}a_m[1-\cos(k_x\cdot m\cdot\Delta x)]\right\}\\&+\frac{v^2\cdot\Delta t^2}{\Delta z^2}\left\{\sum_{m=1}^{M}a_m[1-\cos(k_z\cdot m\cdot\Delta z)]\right\}\end{aligned} \tag{9}$$

To guarantee the stability of the algorithm, set that $\sin^2\left(\frac{\omega\cdot\Delta t}{2}\right)\le 1$. Thus equation 9 must satisfy the following equation:

$$\begin{aligned}&\frac{v^2\cdot\Delta t^2}{\Delta x^2}\left\{\sum_{m=1}^{M}a_m[1-\cos(k_x\cdot m\cdot\Delta x)]\right\}+\\&\frac{v^2\cdot\Delta t^2}{\Delta z^2}\left\{\sum_{m=1}^{M}a_m[1-\cos(k_z\cdot m\cdot\Delta z)]\right\}\le\frac{1}{2}\end{aligned} \tag{10}$$

For a_m appears plus-minus alternately, $\sum_{m=1}^{M} a_m[1-\cos(k_x \cdot m \cdot \Delta x)]$ and $\sum_{m=1}^{M} a_m[1-\cos(k_z \cdot m \cdot \Delta z)]$ reach maximum when horizontal wave number k_x and vertical wave number k_z equal $\frac{\pi}{\Delta x}$ and $\frac{\pi}{\Delta z}$ separately. Thus equation 10 can be simplified as:

$$v_{\max}\Delta t\sqrt{\frac{1}{\Delta x^2}+\frac{1}{\Delta z^2}} \le \frac{1}{2\sqrt{\sum_{m=1}^{M_1} a_{2m-1}}} \tag{11}$$

Commonly, the minimum $\min(\Delta x, \Delta z)$ between Δx and Δz is used to further simplify the equation above as:

$$\frac{v_{\max}\Delta t}{\min(\Delta x,\Delta z)} \le \frac{1}{\sqrt{2\sum_{m=1}^{M_1} a_{2m-1}}} = s \tag{12}$$

where M_1 represents the max odd number which is not bigger than M, $v_{\max}(x, z)$ is the max velocity of medium.

The stability conditions of difference scheme of different precision are listed in the following table:

Table 1
The Stability Condition of 2M-Order Finite Difference Scheme

Precision (2M order)	S
2	0.7071
4	0.6124
6	0.5752
8	0.5546
10	0.5413
20	0.5105
…	…
∞	0.4502

Analyzing the table above, several conclusions can be achieved. Do discretization to spatial differential coefficient, when discrete scheme is 2, 4, 8 or 10 order precision, the corresponding s in stability condition is 0.7071, 0.6124, 0.5752 or 0.5413 separately. Thus, when promoting precision by using high-order difference, the corresponding stability condition is getting higher. When finite difference has infinite order, s approaches 0.4502. For the max velocity in interested area, spatial step length must be chosen adequately when building velocity model. It is also necessary to chose time-step length properly to make it satisfy the stability condition. For we use temporal second order and spatial 10-order difference scheme in this paper, the following equation must be satisfied:

$$\frac{v_{\max}(x,z)\cdot\Delta t}{\Delta x} \le 0.5413 \tag{13}$$

1.4 Frequency Dispersion

Frequency dispersion is the phenomenon that seismic wave disperses with the increment of time which is caused by the different transmitting velocity of waves of different frequency. The frequency dispersion phenomenon caused by grid discretization is called grid frequency dispersion. This phenomenon happens for grid discretization causes some error inevitably when using finite difference method to do difference discretization to wave equation. Grid frequency dispersion is related to velocity, main frequency and grid interval. Generally, the bigger the grid interval is, the heavier the frequency dispersion will be. However, it is unrealistic minimizing grid interval to make the frequency dispersion lowered. There are several principles to realize it:

Use high order difference which can reduce frequency dispersion effectively. Its disadvantage is the increment of the amount of calculation.

Reduce grid interval properly, and its disadvantage is the increment of calculation points and the amount of calculation.

Minimize temporal step length properly.

Do adequate correction to discrete difference arithmetic operator for reducing the error caused by discretization.

1.5 Imaging Condition

McMechan concluded three imaging conditions for reverse-time migration in 2008[13]:

Excitation time imaging condition. The key point of this imaging condition is that the imaging time of each point in imaging space is the one-way time of direct wave from source to that point.

The ratio of up-going wave amplitude to down-going wave amplitude. Its principle is that the reflection point locates where up-going wave field (source wave field) and down-going wave field (receiver wave field) coincide temporally and spatially.

Cross correlation imaging condition. In this method, imaging section is derived by doing zero-delay cross correlation to forward extrapolated source wave field and reverse-time extrapolated receiver wave field.

In this paper, we choose cross correlation imaging condition. For each single-shot gather, cross correlation imaging condition can be expressed as:

$$I(x,z) = \int_0^{tmax} S(x,z,t)R(x,z,t)dt \tag{14}$$

where x and z represent horizontal and vertical coordinates separately, t represents time, S(x,z,t) represents source wave field, and R(x,z,t) represents receiver wave field.

1.6 Migration Noise

In reverse-time migration, using imaging relation $t_s+t_r=t$ to extract imaging value, reverse-time migration ray will reflect at the hard interface of the velocity model. Thus every point along reflection path satisfies the equation

$t_s+t_r=t$ as is shown in the following figure (the locations indicated by the pane and the ellipse). Therefore, despite the imaging of true subsurface interfaces, reverse-time migration produces a mass of pseudomorphous results.

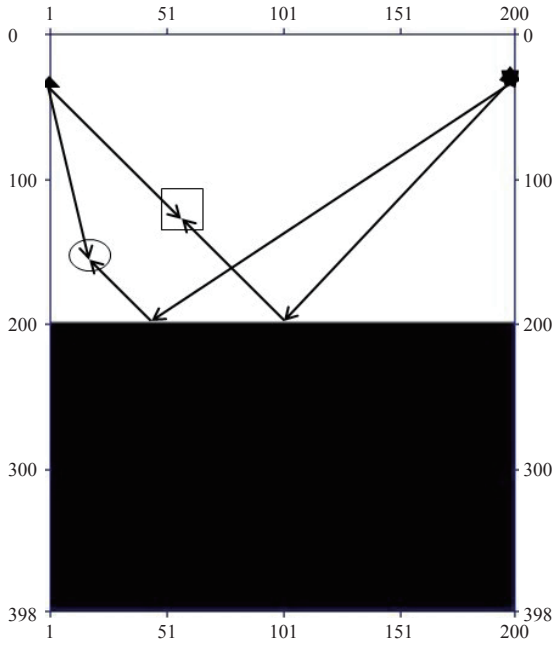

Figure 1
The Mechanism of Low Frequency Noise of Cross-Hole Seismic

For reducing low-frequency noise, Laplacian filter method is used in paper. According to Laplacian filter method[14], wave number vector algorithm and cosine theorem, we can derive equation:

$$k_x^2+k_y^2+k_z^2=4\frac{\omega^2}{v^2}\cos^2\theta \tag{15}$$

So Laplacian filter is equavalent to angle-domain filter. It reduces imaging noise while reserving useful imaging results partially.

2 MODEL TEST

2.1 A Model with Anomalous Ellipsoids

As is shown in the following figure (Figure 2), we use a geological model with subsurface anomalous ellipsoids to introduce how the suitability of reverse-time migration varies with the change of anomalous body velocity. In the model, the velocity of the upper layer is 3500 m/s, the velocity of the underlying layer is 4000 m/s, and the velocity of anomalous ellipsoids is 2500 m/s. The diameters of the two ellipsoids are 10 m and 15 m separately. The size of the model is 111 m×401 m, and the size of grid is 1 m×1 m. The left well is excitation well, and source depth varies from 1 m to 391 m. Shot interval is 10 m, and shot number is 40. The right well is observation well, and receiver depth varies from 1 m to 401 m. Trace interval is 1 m. In forward modeling, we use Ricker wavelet as source wavelet whose main frequency is 150 Hz.

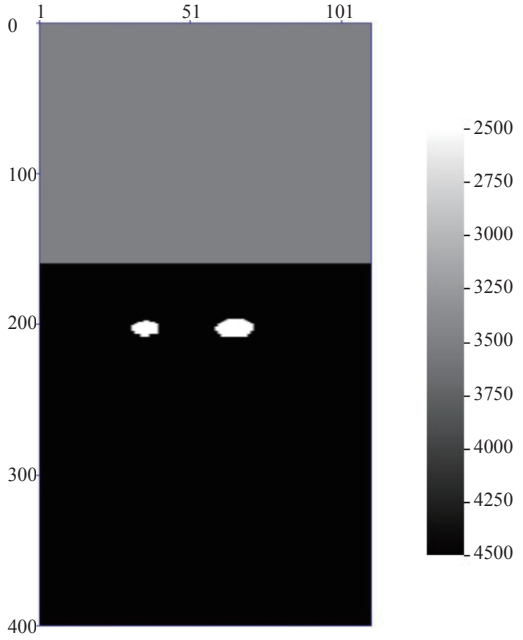

Figure 2
A Model with Anomalous Ellipsoids

The migration result of 40 shots is shown in Figure 3. With the comparison to velocity section, obviously, horizontal interface and the two underlying anomalous ellipsoids are imaged.

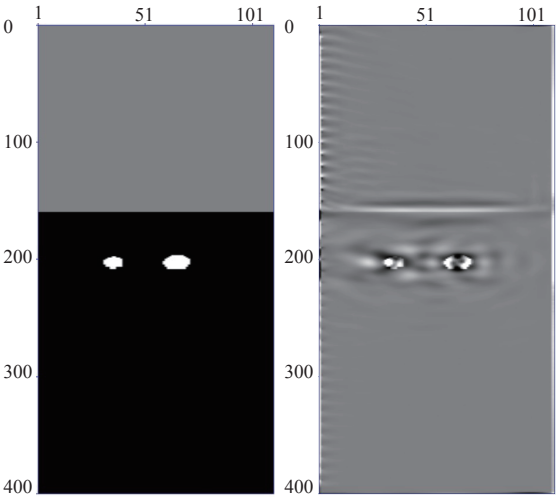

(a) Velocity Model (b) RTM Section

Figure 3
The Comparison of Velocity Model and RTM Section

Figure 4 shows a complex model whose size is 1001 m×2001 m. Grid size is 1 m×1 m. The left well is excitation well while the right well is observation well. Source depth varies from 686 m to 1817 m. Shot interval is 3 m, and shot number is 378. Receiver depth

varies from 950 m to 1649 m, and trace interval is 3 m. In the process of migration, we use Ricker wavelet as source wavelet whose main frequency is 150 Hz. With the comparison to velocity section, the upper horizontal layer and the underlying three velocity-anomalous bodies are imaged clearly, and the deep-seated three rounded anomalous bodies and protuberant parts of the interface are also imaged apparently.

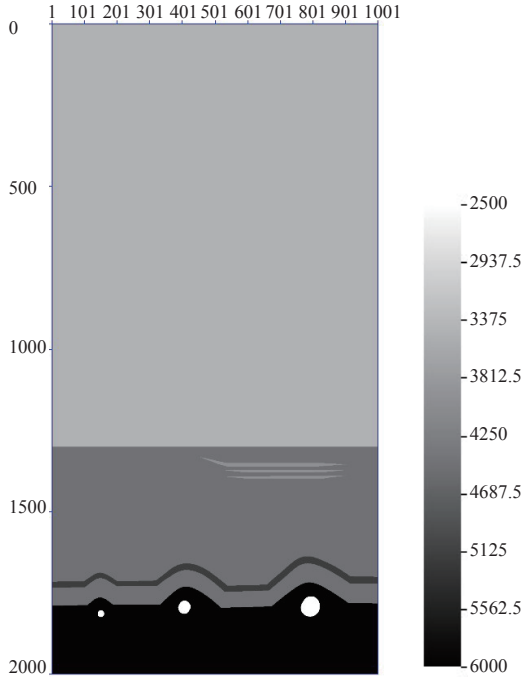

Figure 4
Complex Model

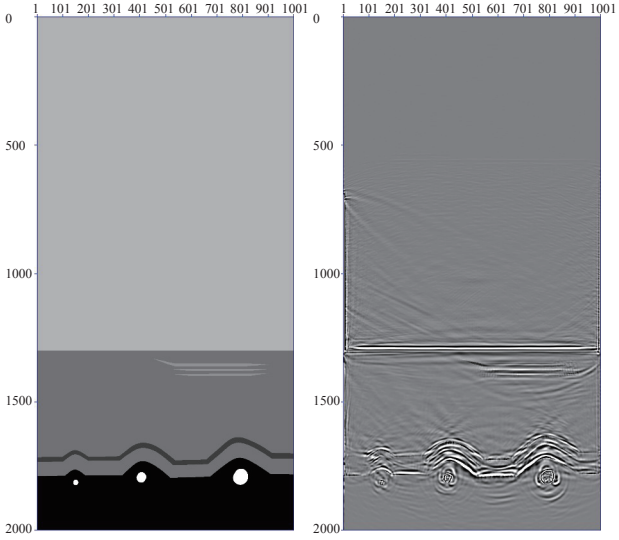

(a) Velocity Model (b) RTM Section

Figure 5
The Comparison of Velocity Model and RTM Section

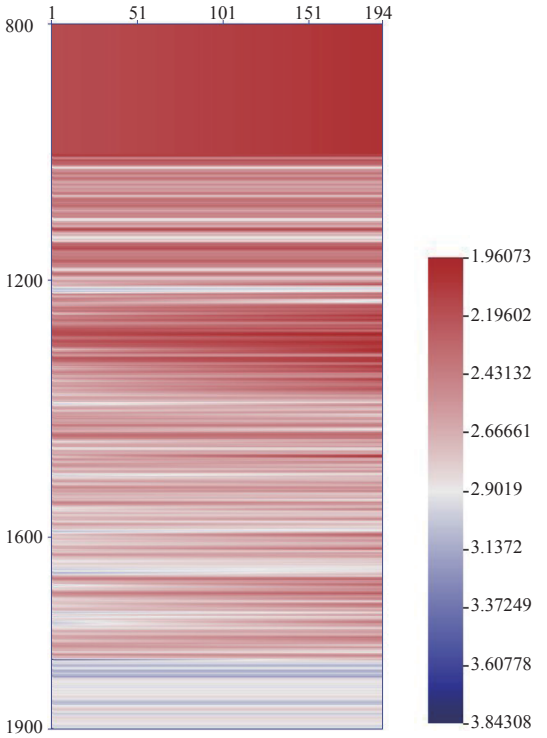

Figure 6
Velocity of Cross-Hole Seismic

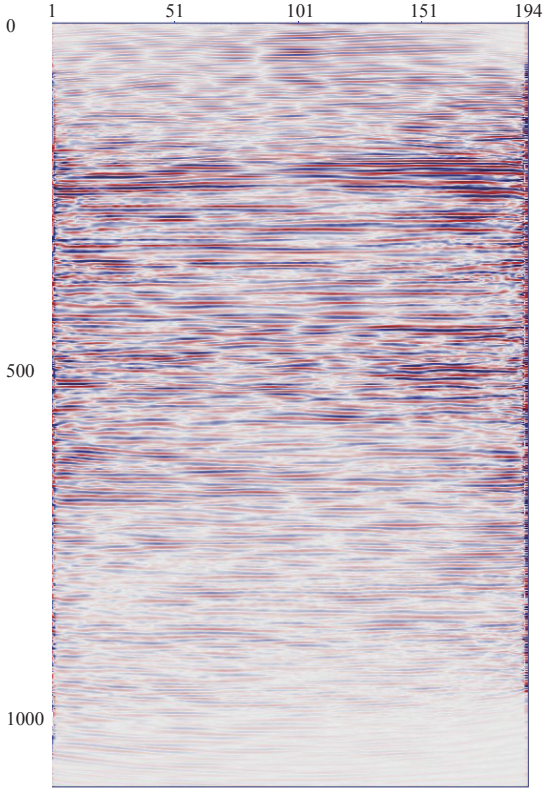

Figure 7
RTM Section Based on Cross-Hole Seismic Data

We process a real connected-well data of Shengli Oil Field to test the effectiveness of reverse-time migration for real data. Applying interpolation to logging data, we derive the velocity field as is shown in Figure 6 (the unit is km/s). The size of the model is 194 m×1101 m, and the size of grid is 1 m×1 m. The depth range of velocity field is 800 m-1900 m. The left well is excitation well, and source depth varies from 852 m to 1848 m. Shot interval is 3 m, and shot number is 333. The right well is observation well. Receiver depth varies from 861 m to 1758 m, and receiver interval is 3 m.

Figure 7 shows the cross-hole seismic migration section. Figure 8 is the partial enlarged detail of migration section. The imaging section reflects the thin-interbed feature of the stratum. The continuity of seismic events is good. Thus the migration result is consistent with real geological situation.

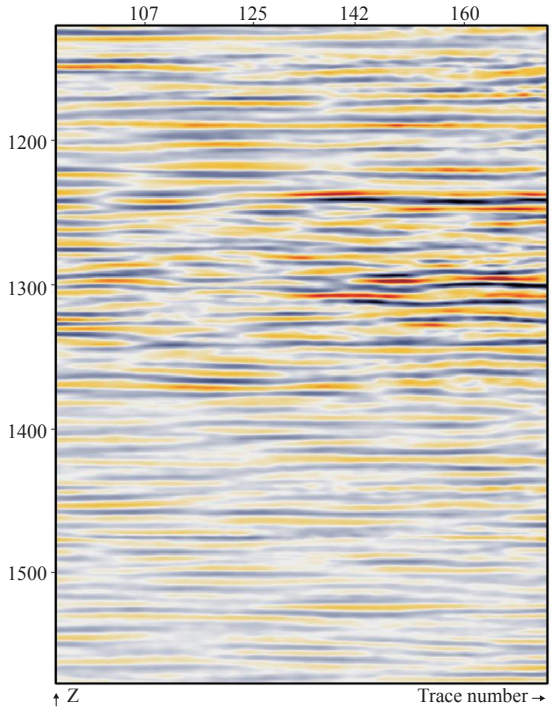

Figure 8
Partial Enlarged Detail of RTM Section

CONCLUSION

In this paper, cross-hole seismic reverse-time migration method is discussed. We put forward a difference operator for forward and reverse-time extrapolation, derive the stability condition of difference scheme, and propose the principle of choosing grid size when building velocity model. The work in model test demonstrates the imaging ability of cross-hole reverse-time migration. When dealing with real data, for cross-hole seismic data has higher frequency, the final imaging section has a higher resolution, being able to distinguish thin layer, and the continuity of seismic events in imaging section is relatively good.

REFERENCES

[1] Whitmore, N. D. (1983). Iterative Depth Migration by Backward Time Propagation. *1983 SEG Annual Meetin*g, September 11 - 15, Las Vegas, Nevada.

[2] Levin, S. A. (1984). Principles of Reverse Time Migration. *Geophysics*, *49*(5), 581-583.

[3] Hildebrand, S. T. (1987). Reverse Time Depth Migration: Impedance Imaging Condition. *Geophysics*, *52*(8), 1060-1064.

[4] Chang, W. F., & McMechan, G. A. (1989). 3D Acoustic Reverse-Time Migration. *Geophysical Prospecting*, *37*(3), 243-256.

[5] Zhang, Y., & Sun, J. (2008). Practical Issues of Reverse Time Migration: True-Amplitude Gathers, Noise Removal and Harmonic-Source Encoding. *EAGE Conference & Exhibition*.

[6] Zhu, X. H., & Mcmechan, G. A. (1988). Acoustic Modeling and Migration of Stacked Cross-Hole Data. *Geophysics*, *4*(53), 492-500.

[7] Balch, A. H., et al. (1991). Use of Forward and Bac-Scattered P and S Wave Converted Waves in Cross-Blrehole Imaging. *Geophysical Prospecting*, *7*(39), 887-913.

[8] Xin, Z. (1996). *Methods Research of Reflection Wave Prestack Depth Migration in Crosswell Seismic* (Doctoral dissertation). China University of Petroleum.

[9] Yan, H. S. (2009). *3C Borehole Seismic Data Wavefield Separation and Application* (Doctoral dissertation). China University of Petroleum (East China).

[10] Ping, Y. F. (2011). *Crosswell P Wave and S Wave Imaging and Application* (Doctoral dissertation). China University of Petroleum (East China).

[11] Soubaras, R., Zhang, Y., & Veritas, C. G. G. (2008). Two-Step Explicit Marching Method for Reverse Time Migration. *2008 SEG Annual Meeting*, November 9 - 14, Las Vegas, Nevada.

[12] Liu, Y., & Wei, X. C. (2008). Finite-Difference Numerical Modeling with Even-Order Accuracy in Two-Phase Anisotropic Media. *Applied Geophysics*, *5*(2), 107-114.

[13] Chattopadhyay S., & Mcmechan, A. G. (2008). Imaging Conditions for Prestack Reverse-Time Migration. *Geophysics*, *3*(73), S57-S66.

[14] Yan, C. Z., Chun, Z. L., & Dong, X. S. (2010). Review of Reverse Time Migration. *Progress in Exploration Geophysics*, *5*(33), 309-317.